Virtual and Physical Prototyping 2016 (Accepted version)

Fabrication of heat sinks by Selective Laser Melting for convective heat transfer applications

In this paper, the forced convective heat transfer performance of heat sinks produced by Selective Laser Melting (SLM) was experimentally investigated. Three heat sinks comprising pin fins of circular, rectangular-rounded and aerofoil geometries were fabricated by SLM from aluminium alloy AlSi10Mg powder. The heat sinks were tested in a rectangular air flow channel for convective heat transfer performance. Experiments performed for Reynolds numbers ranging from 3400 to 24,000 show that the heat transfer performances of the aerofoil and rectangular rounded heat sinks exceeded those of the circular heat sink. Using the cylindrical heat sink as a benchmark, the average enhancements in the normalised Nusselt numbers were computed to be 15.0% and 21.4% for the rectangular rounded and aerofoil heat sinks, respectively. It was demonstrated that SLM can be employed to design and fabricate heat sinks of customised geometries for heat sink applications.

Keywords: Selective Laser Melting; AlSi10Mg; heat sink; aerofoil; convective heat transfer

1. Introduction

Selective Laser Melting (SLM) is an additive manufacturing technique to produce solid metal parts from the melting of metal powders in a layer-by-layer fashion (Chua et al. 2014). The as-built parts can be near 100% relative density and this is typically used as a criterion for quality. Many materials can be processed using SLM, such as stainless steel, Inconel, titanium and aluminium alloys (Abe et al. 2001). The ability to manufacture complex internal geometries is one major advantage which conventional manufacturing cannot replicate (Yan & Gu 1996). Another advantage of SLM is that the built part can be near net shape and eliminates the need for a mould or long post-processing methods, as often required in casting. This greatly reduces the production cost for small volumes of highly customised parts (Read et al. 2015; Yadroitsev et al.

2015).

Several researchers have attempted to incorporate SLM in the fabrication of heat sinks. Heat sinks are passive devices which make use of extended surfaces to increase heat dissipation from a heat source to the surroundings. SLM shows potential for fabricating heat sinks as it is able to process metals such as aluminium alloys which have high thermal conductivity and is also able to produce parts of high relative density. The processing parameters of aluminium alloys have been investigated by many researchers, such as that of AlSi10Mg (Brandl et al. 2012; Kempen et al. 2012; Thijs et al. 2013; Aboulkhair et al. 2014; Li and Gu 2014; Lam et al. 2015), Al6061 (Loh et al. 2014, 2015) and AlSi12 (Louvis et al. 2011).

Wong et al. (2007) investigated air-cooling of heat sinks circular, elliptical and V-shaped geometries fabricated from Al6061 using SLM. A heat sink comprising fins with circular geometry was also fabricated using SLM from stainless steel 316L. It was shown that the higher thermal conductivity of Al6061 as compared to stainless steel 316L produced better heat transfer performance. Wong et al. (2009) further fabricated heat sinks with fins of rectangular, rectangular-rounded and lattice-type geometries using SLM from Al6061. It was found that both the rectangular and rectangular-rounded fins have better heat transfer performance, but the lattice-type fins performed poorly due to the struts being too thin and resulting in poor fin efficiency. However, for both experiments, the processing parameters for Al6061 used only managed to achieve a maximum relative density of 90%. Neugebauer et al. (2011) produced a miniature water-cooled heat exchanger using SLM and demonstrated that new design approaches can be made to improve efficiency by additive manufacturing. The fine details and close proximity of the parts produced by SLM showcased the process' ability to manufacture high surface-volume ratio heat sinks with intricate and complex designs. Ventola et al.

(2014) used the direct metal laser sintering technique to fabricate heat sinks of different artificial surface roughness. It was observed that a maximum heat transfer enhancement of 73% was achieved in a rough sample surface as compared to that of a smooth surface.

For air-cooled heat transfer devices, pin fin arrays are commonly used. The fins can have cross sectional areas varying from circular, elliptical, square to rectangular shapes. Due to the flexibility in changing the designs of pin fin heat sinks by simply varying the cross sectional area of the pins, much research have been carried out to determine the performance of different designs of pin fins. Li & Kim (2008) conducted numerical studies to optimise staggered elliptical pin fin arrays. Sahiti et al. (2006) and Zhou & Catton (2011) conducted numerical studies on a variety of cross-section shapes viz. circular, square, elliptical, NACA aerofoil, dropform and lancet. Chen et al. (1997) showed that the streamline profile of drop-shaped fins resulted in better heat transfer than circular fins and much lower air resistance.

In many practical applications, the heat sinks are often exposed or exist in conditions where they are not fully enclosed in a duct. The existence of clearances around the heat sinks may result in air bypassing the fins due to air resistance. This typically reduces the air flow through the fins and affects heat sink performance. The objectives of this paper are to demonstrate the ability of using SLM to produce heat sinks of high density and good dimensional accuracy, and to characterise their convective heat transfer performances. The fabrication of novel heat sink with fins of aerofoil geometry for convective heat transfer applications will be investigated in a vertical channel which has large clearance to allow air bypass, so as to simulate practical applications. The results will be compared with that of circular and rectangular-rounded geometries fabricated using SLM. The superior heat transfer

performance of the aerofoil fins will be highlighted, which can be attributed to having a streamline shape which resulted in lower air bypass.

2. Methodology

2.1. Equipment and materials

The machine used is SLM250HL (SLM Solutions GmbH), which is housed in the Future of Manufacturing Laboratory 1 of the Singapore Centre for 3D Printing (SC3DP) at Nanyang Technological University. A Gaussian distributed Yb:YAG laser of maximum power of 400 W and laser beam spot size of 80 μm was used for melting the metal powder. During the manufacturing process, the build chamber is flushed with argon gas until the oxygen level is lower than 0.2%, so as to minimise oxidation and combustion.

The powder is first distributed evenly on a substrate base plate. The Yb:YAG laser is used to provide the high energy densities necessary for complete melting. The laser scanning melts the powder according to a pre-programmed pathway that is defined in Computer Aided Design (CAD) file. The powder layer is rapidly melted and then solidified to form a thin solid layer. The powder bed is then lowered by one layer and re-deposited. Laser scanning subsequently melts and bonds the new layer to the previous layer. This process is repeated until the entire part is formed.

The composition of the AlSi10Mg powder used, as provided by the supplier, is listed in Table 1. Spherical AlSi10Mg powder with a distribution size of 20 μm to 63 μm was used. The Scanning Electron Microscope (SEM) image of the powder at a magnification of 300 times is shown in Figure 1.

For this paper, the layer thickness was set at 50 μm. The laser beam power was 350 W, laser scan speed was 1150 mm/s and hatch spacing was 170 μm. The parameters

were tested by Sing et al. (2015) for AlSi10Mg and were shown to produce parts of high density. The parallel line scanning method was chosen with rotation of 30° for every layer to obtain final samples with isotropic properties. Prior to the fabrication of the heat sinks, three cubes of 1 cm^3 volume were fabricated using the above-mentioned parameters and the relative densities were evaluated using Archimedes' principle on a XSE204 Analytical Balance from Mettler-Toledo. High relative density of average 99.1% was obtained, which demonstrated that the processing parameters were suitable for the AlSi10Mg powder.

2.2. Fabrication of heat sinks

Three heat sinks of staggered arrangements, namely circular, rounded rectangular and aerofoil (NACA-4424) geometries were fabricated using SLM. The base area (A_b) of the heat sinks is 2500 mm^2 with dimensions of 50 mm by 50 mm, and a thickness of 5 mm. The fin height was fixed at 25 mm. For the circular arrangement, it consisted of 41 fins, each with diameter of 4 mm and fin spacing of 10 mm. For the rectangular-rounded arrangement, the array consists of 41 fins of 2 mm width and 6 mm length each. For the aerofoil arrangement, it consists of 23 NACA-4424 fins, with a maximum thickness at 2.4 mm and chord length of 10 mm. The fabricated heat sinks are shown in Figure 2. The total wetted surface area (A_t) is defined as the surface area which is in contact with the air during convection. The parameters for the heat sinks are summarised in Table 2.

2.3. Heat transfer experimental setup

The convective heat transfer experiments were conducted by providing air flow over the heat sinks in a vertical channel which has a total length of 1000 mm, from the air flow inlet to the fan discharge. The channel has a cross-sectional area of 127.5 mm by 75 mm and the hydraulic diameter (D_H) is computed to be 94.4 mm. The cross-sectional area of

the channel is large compared to the heat sink cross-sectional area of 50 mm by 25 mm (height of fins) in the direction of air flow, thus allowing bypass of air flow. This was to simulate the common operating conditions where the heat sinks are not fully ducted. An inclined manometer was used to measure the overall system pressure with the pressure port located 650 mm downstream of the inlet. The power to the fan was varied to provide air flow at different speeds. An air flow sensor is positioned at 350 mm from the inlet to obtain the average air velocity (V_{air}). Thermocouples were included at the inlet and outlet regions of the channel to measure the air stream temperatures, T_{in} and T_{out}, respectively. The experimental setup is illustrated in Figure 3.

The heat source for the experiment was provided by four cartridge heaters inserted into a copper block so as to provide uniform heat flux to the surface of the heat sink. The heat sink was attached to the copper block using thermally conductive epoxy, "Omegabond-101" so as to reduce contact resistance. For insulation, 15 mm and 21 mm thick Teflon were used to surround the side and back of the copper block, respectively. The assembly is then fitted into an aluminium holder which is in turn secured onto the bottom side of the air flow channel such that the top surface of the heat sink base plate flushes with the internal channel wall. Finally, a 6-mm-thick foam made of elastomer, which serves as a second layer of insulation, is applied around the aluminium holder. The heat input to the cartridge heaters were varied using a variable transformer. In order to measure the surface temperature of the heat sinks, two holes were drilled from the sides into the base of heat sinks for two thermocouples to be inserted. The average of the two temperatures at the heat sink base, T_w, was used in calculation. The temperatures of the heat sink, inlet and outlet were recorded using the MW100 Data Acquisition Unit.

2.4. Experimental procedures and data reduction

The power to the cartridge heaters can be calculated by the product of current (I) and voltage (V). The power input was set such that it was equal to 15 W. The average heat loss ($\dot{Q}_{loss}$) due to natural convection was estimated to be about 12%. The total heat input ($\dot{Q}$) to the heat sink is shown in Equation (1).

$$\dot{Q} = I \times V - \dot{Q}_{loss} \tag{1}$$

The air speed was varied from 0.5 m/s to 3.5 m/s at intervals of 0.5 m/s. Using Equation (2), the computed Reynolds numbers (Re) lie between 3400 to 24000. For each air speed, the heat sink wall temperature (T_w), air inlet temperature (T_{in}) and outlet temperature (T_{out}) were recorded when steady state condition was reached which was deemed to be reached when the temperature reading fluctuations were within ± 0.1 °C for at least 5 minutes. The waiting time was between 30 minutes and 2 hours for steady state to be achieved. The system pressure was also recorded from the inclined manometer. After completing the above cycle, the experiments were then repeated.

$$Re = \frac{\rho_{air} V_{air} D_H}{\mu_{air}} \tag{2}$$

The heat transfer performance of the different heat sinks was determined in terms of the convective heat transfer coefficient with respect to the base plate area (h_b) and the total wetted surface area (h_t), shown in Equations (3) and (4), respectively.

$$h_b = \frac{\dot{Q}}{A_b[T_w - \left(\frac{T_{out}+T_{in}}{2}\right)]} \tag{3}$$

$$h_t = \frac{\dot{Q}}{A_t[T_w - \left(\frac{T_{out}+T_{in}}{2}\right)]} \tag{4}$$

Using Equations (3) and (4), the Nusselt numbers were computed in Equations (5) and (6).

$$Nu_b = \frac{h_b D_H}{k_{air}} \quad (5)$$

$$Nu_t = \frac{h_t D_H}{k_{air}} \quad (6)$$

The uncertainties of the current and voltage readings from the variable transformer are within ± 0.5% of their full scale whereas the thermocouples were calibrated to within ± 0.5°C deviation for the range of temperatures. The accuracy of the air flow sensor is within ± 3% of its full scale and the inclined manometer has the accuracy of ± 0.5 Pa. Using the method described by Moffat (1985), the average uncertainties of h_b, Nu_b and Re were determined to be 6.6%, 6.6% and 7.8%, respectively and the maximum uncertainties of h_b, Nu_b and Re are 7.5%, 7.5% and 21%, respectively.

3. Results and discussions

3.1. Dimensional and surface measurement of heat sinks

Dimensional accuracy of the printed parts was determined by taking microscopic measurements of the fins. An "OLYMPUS" SZX7 Zoom Stereo Microscope was used in this process. Twenty fins of each heat sink were randomly chosen and their dimensions were measured and their average values were computed. The close-up images of the different heat sinks are shown in Figure 4. From the measurements taken, the maximum dimensional error of the fins is 2.5%. For the diameter of the circular cross-section (4 mm), length of the rounded rectangular cross-section (6 mm) and chord of the aerofoil cross-section (10 mm), the dimensional errors are 2.4%, 1.1% and 2.4%,

respectively. The analyses showed that SLM is able to fabricate small and intricate components accurately with only a small dimensional error.

Conventional manufacturing methods of heat sinks include extrusion, die-casting, bonding, brazing and machining. Compared to bonding and brazing methods where the fins are joined to the base using a conductive epoxy or solder, SLM eliminates the thermal contact resistance between the fins and base by fabricating the heat sinks in entirety. The fabrication of aerofoil fins by casting or machining methods is difficult due to its complex geometry. This is where SLM shows the feasibility of design and fabrication of customised geometries for heat sink applications. The designs can be quickly iterated and many combinations can be produced for testing to investigate the optimal parameters. This would be difficult to achieve in conventional manufacturing methods where tooling costs and lag time are more significant.

3.2. Effects of geometry on heat transfer performance

The convective heat transfer performances of the cylindrical, rectangular-rounded and aerofoil heat sinks are compared using the Nu_b at different Re, as shown in Figure 5. The aerofoil and rounded-rectangular heat sinks performed better than the cylindrical heat sink. At low Re, the aerofoil and rounded-rectangular heat sinks are of comparable performance. The performance of rounded-rectangular increased almost linearly with increasing Re, however while the performance of aerofoil heat sink increased with increasing Re, the rate of increase actually decreased with increasing Re. In order to evaluate the overall performances of the heat sinks, the average Nu_b of the respective heat sinks were calculated for the range of Re tested. Overall, using the cylindrical heat sink as a benchmark, the average enhancements in Nu_b are computed to be 28.1% and 16.4% for the rectangular-rounded and aerofoil heat sinks, respectively.

As shown in Table 2, the heat sinks possess different total wetted surface areas (A_t) due to the differences in fin geometries. In order to account for the area differences, the heat transfer performance is compared using the normalised Nusselt numbers (Nu_t) which accounts for the total wetted surface area, as shown in Equations (4) and (6). The Nu_t of the different heat sinks corresponding to the various Re are plotted in Figure 6 for comparison. The heat transfer performances of both aerofoil and rectangular-rounded heat sinks are still to be better than the cylindrical heat sinks. However, it can be observed that the aerofoil heat sink performed better than the rectangular rounded heat sink at low Re, and the performance of rectangular-rounded heat sink appears to surpass the aerofoil heat sink at high Re. Using the cylindrical heat sink as a benchmark, the average enhancements in Nu_t are computed to be 15.0% and 21.4% for the rectangular-rounded and aerofoil heat sinks, respectively.

3.3. Heat transfer enhancement mechanisms

The aerofoil heat sink is a more streamline geometry as compared to the circular and rectangular-rounded heat sinks, which allows a lower air resistance. From the pressure readings, all three heat sinks possess negligible pressure drops of less than 5 Pa due to the large area of bypass in the experimental setup. Hence, for the same Re, the aerofoil heat sink resulted in minimal air bypass and enabled higher air flow rate through the heat sink, which in turn increased the heat removal rate and explains the highest Nu_t amongst all the heat sinks at low Re.

However, as air flow velocity increases with increasing Re, due to the blunt edges of the rounded rectangular heat sink, vortices were likely to be formed at the trailing edge of the fins which induced fluid mixing and further enhanced heat transfer. Figure 7 illustrates the formation of vortices on the trailing edge of the rectangular rounded fin in a mini smoke wind tunnel, where the air speed is at 1.5 m/s. The heat

transfer enhancement due to the effect of vortex formation is likely to surpass that of higher air flow experienced by the aerofoil heat sink at high Reynolds number.

3.4. Challenges to fin optimisation in heat sink designs

The challenges to the optimisation of fin design lie in the multitude of parameters present, such as the fin geometry, fin dimensions, fin arrangement and material used. Apart from the heat transfer performance, the pressure drop characteristics of heat sinks need to be considered as it will affect the cost of pumping power. In a practical situation where the heat sinks are not fully enclosed in a duct, the clearance present will affect the amount of air bypass and heat transfer performance too. For instance, Sparrow et al. (1978) conducted convective heat transfer experiments on fin arrays with small fin spacing in the presence of tip clearance, and it was observed that heat transfer increases near the fin tip.

By employing SLM, it is possible to quickly design and fabricate heat sinks of novel designs for experimental testing. Moreover, it is possible to customise staggered heat sinks with different fin densities, orientations and geometries to maximise heat transfer while keeping low pressure drop.

4. Conclusions

In this paper, three heat sinks with fins of circular, rectangular-rounded and aerofoil (NACA442) geometries were fabricated using the SLM technique and experimentally investigated in a vertical channel for convective heat transfer performances. The vertical channel has large clearance to allow air bypass so as to simulate practical applications where the heat sinks are not fully enclosed in a duct. The heat sinks possess high relative density of 99.1%, good dimensional accuracy and demonstrated the ability of SLM to produce fins of unique geometries. Using the cylindrical heat sink as a

benchmark, the average enhancements in Nu_t are computed to be 15.0% and 21.4% for the rectangular rounded and aerofoil heat sinks, respectively. The enhancements are attributed to the streamline nature of aerofoil heat sink which allows less bypass and the formation of vortices for the rectangular rounded heat sink which allows better fluid mixing. SLM has been demonstrated to be feasible for design and fabrication of customised geometries for heat sink applications. Future work will be conducted to investigate the optimal parameters in terms of the fin geometries and arrangements for high heat transfer performances and low pressure drop.

Acknowledgments

The authors will like to acknowledge the assistance of Mr. Lim Ming Chong in conducting some of the experiments reported in this paper and the National Research Foundation, Singapore for funding of the SLM facilities.

References

Abe, F., Osakada, K., Shiomi, M., Uematsu, K., and Matsumoto, M., 2001. The manufacturing of hard tools from metallic powders by selective laser melting. *Journal of Materials Processing Technology*. 111(1–3), 210-213.

Aboulkhair, N.T., Everitt, N.M., Ashcroft, I. and Tuck, C., 2014. Reducing porosity in AlSi10Mg parts processed by selective laser melting. *Additive Manufacturing*, 1, 77-86.

Brandl, E., Heckenberger, U., Holzinger, V. and Buchbinder, D., 2012. Additive manufactured AlSi10Mg samples using Selective Laser Melting (SLM): Microstructure, high cycle fatigue, and fracture behavior. *Materials & Design*, 34, 159-169.

Chen, Z., Li, D., Meier, D., Warnecke, H.-J., 1997. Convective heat transfer and pressure loss in rectangular ducts with drop-shaped pin fins, *Heat and Mass Transfer*, 33, 219-224.

Chua, C.K. and Leong, K.F., 2014. *3D Printing and Additive Manufacturing: Principles and Applications*. 4th ed. Singapore: World Scientific Publishing Co. Pte. Ltd.

Kempen, K., Thijs, L., Van Humbeeck, J., and Kruth, J.P., 2012. Mechanical properties of AlSi10Mg produced by Selective Laser Melting. *Physics Procedia*, 39, 439-446.

Lam, L.P., Zhang, D.Q., Liu, Z.H. and Chua, C.K., 2015. Phase analysis and microstructure characterisation of AlSi10Mg parts produced by Selective Laser Melting. *Virtual and Physical Prototyping*, 10(4), 207-215.

Li, Y. and Gu, D., 2014. Parametric analysis of thermal behavior during selective laser melting additive manufacturing of aluminum alloy powder. *Materials & Design*, 63, 856-867.

Li, P., and Kim, K., 2008. Multiobjective optimisation of staggered elliptical pin-fin arrays, *Numerical Heat Transfer*, 53, 418-431.

Loh, L.E., Chua, C.K., Yeong, W.Y., Song, J., Mapar, M., Sing, S.L., Liu, Z.H. and Zhang, D.Q., 2015. Numerical investigation and an effective modelling on the Selective Laser Melting (SLM) process with aluminium alloy 6061. *International Journal of Heat and Mass Transfer*, 80, 288-300.

Loh, L.E., Liu, Z.H., Zhang, D.Q., Mapar, M., Sing, S.L, Chua, C.K., & Yeong, W.Y., 2014. Selective Laser Melting of aluminium alloy using a uniform beam profile, *Virtual and Physical Prototyping*, 9:1, 11-16.

Louvis, E., Fox, P., and Sutcliffe, C.J., 2011, Selective Laser Melting of aluminium components, *Journal of Materials Processing Technology*, 211(2), 275-284.

Moffat, R.J., 1985. Using uncertainty analysis in the planning of an experiment, *Journal of Fluids Engineering*, 107,173-178.

Neugebauer, R., Müller, B., Gebauer, M., and Töppel, T., 2011. Additive manufacturing boosts efficiency of heat transfer components. *Assembly Automation*, 31(4), 344-347.

Read, N., Wang, W., Essa, K., and Attallah, M.M., 2015. Selective Laser Melting of AlSi10Mg alloy: process optimisation and mechanical properties development, *Materials and Design*, 65, 417-424.

Sahiti, N., Lemouedda, A., Stojkovic, D., Durst, F., and Franz, E., 2006. Performance comparison of pin fin in-duct flow arrays with various pin cross-sections, *Applied Thermal Engineering*, 26, 1176-1192.

Sing, S.L., Lam, L.P., Zhang, D.Q., Liu, Z.H. and Chua, C.K., 2015. Interfacial characterization of SLM parts in multi-material processing: Intermetallic phase formation between AlSi10Mg and C18400 copper alloy. *Materials Characterization*, 107, 220-227.

Sparrow, E.M., Baliga, B.R., Patankar, S.V., 1978. Forced convection heat transfer from a shrouded fin array with and without tip clearance, *Journal of Heat Transfer*, 100, 572-579.

Thijs, L., Kempen, K., Kruth, J.P. and Van Humbeeck, J., 2013. Fine-structured aluminium products with controllable texture by selective laser melting of pre-alloyed AlSi10Mg powder. *Acta Materialia*, 61(5), 1809-1819.

Ventola, L., Robotti, F., Dialameh, M., Calignano, F., Manfredi, D., Chiavazo, E., Asinari, P., 2014. Rough surfaces with enhanced heat transfer of electronic cooling by direct laser sintering, *International Journal of Heat and Mass Transfer*, 75, 58-74.

Wong, M., Tsopanos, S., Sutcliffe, C.J. and Owen, I., 2007. Selective laser melting of heat transfer devices. *Rapid Prototyping Journal*, 13(5), 291-297.

Wong, M., Owen, I., Sutcliffe, C.J., and Puri, A., 2009. Convective heat transfer and pressure losses across novel heat sinks fabricated by Selective Laser Melting. *International Journal of Heat and Mass Transfer*, 52(1-2), 281-288.

Yadroitsev, I., Krakhmalev, P., and Yadroitsava, I., 2015. Hierarchical design principles of Selective Laser Melting for high quality metallic objects, *Additive Manufacturing*, 7, 45-56.

Yan, X. and Gu, P., 1996. A review of rapid prototyping technologies and systems. *Computer-Aided Design*, 28(4), 307-318.

Zhou, F., and Catton, I., 2011. Numerical evaluation of flow and heat transfer in plate-pin fin heat sinks with various pin cross-sections, *Numerical Heat Transfer*, 60, 107-128.

Table 1. Composition of AlSi10Mg alloy (%) used.

Al	Si	Fe	Cu	Mn	Mg	Ni	Zn	Pb	Sn	Ti
Balance	9.0-11.0	0.55 max	0.05 max	0.45 max	0.2-0.45	0.05 max	0.10 max	0.05 max	0.05 max	0.15 max

Table 2. Summary of parameters of heat sinks fabricated

Cross-section	Dimensions	Number of fins	Total wetted surface area (A_t)
Circular	• Diameter: 4 mm	41	15380 mm^2
Rounded Rectangular	• Total length: 6 mm • Straight length: 4 mm • Rounded edge diameter: 2 mm • Width: 2 mm	41	17140 mm^2
Aerofoil NACA-4424	• Chord length: 10 mm • Thickness: 2.4 mm	23	14750 mm^2

Figure 1. SEM image of AlSi10Mg powder at a magnification of 300 times.

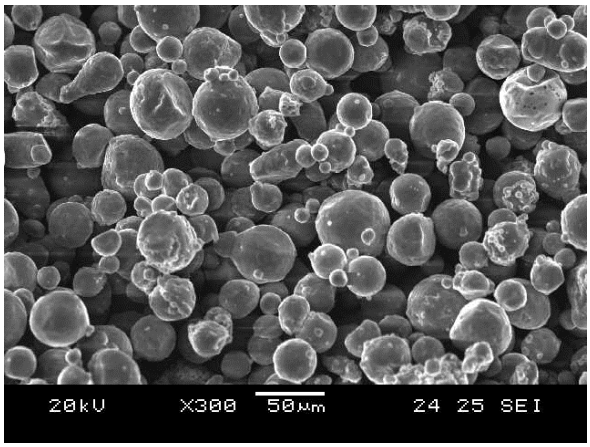

Figure 2. Fabricated heat sinks of (a) circular, (b) rectangular rounded and (c) aerofoil fins.

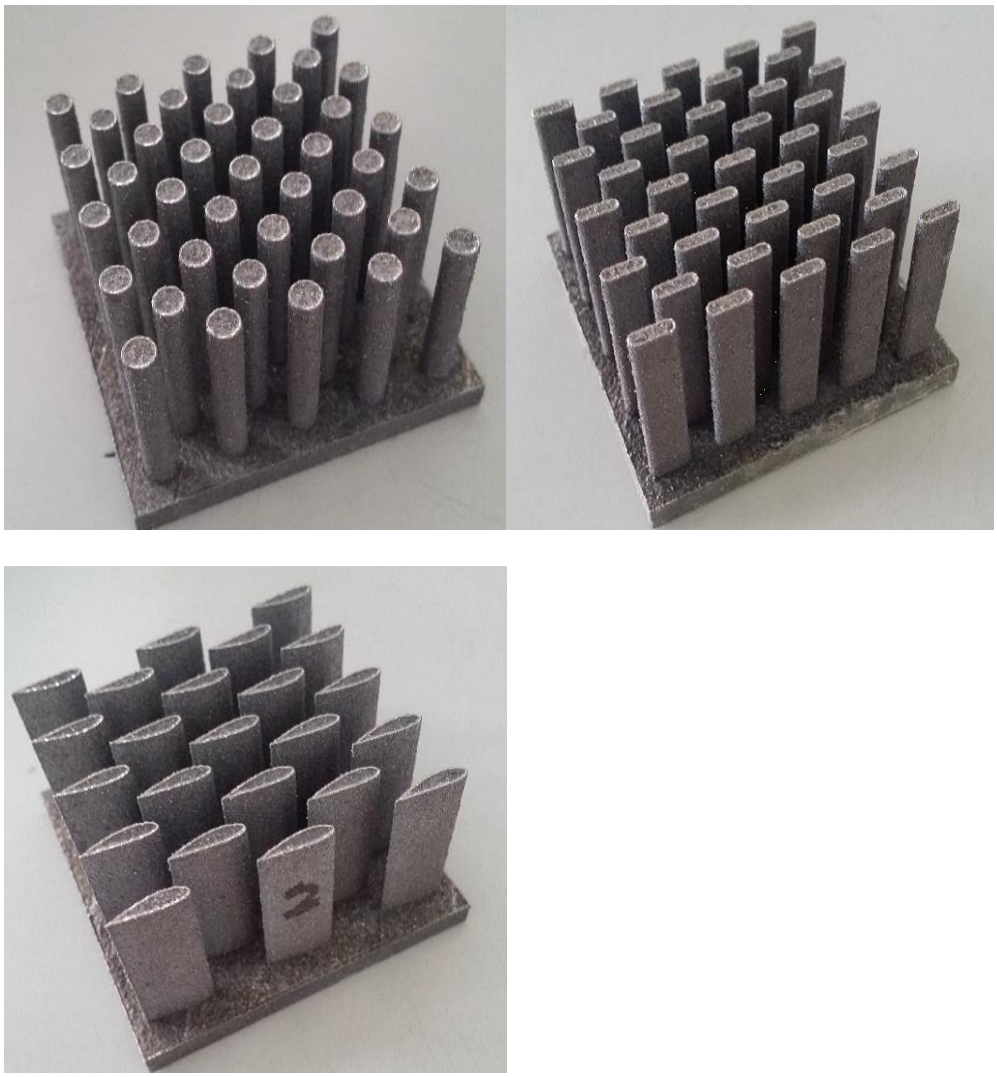

Figure 3. Schematic diagram of setup.

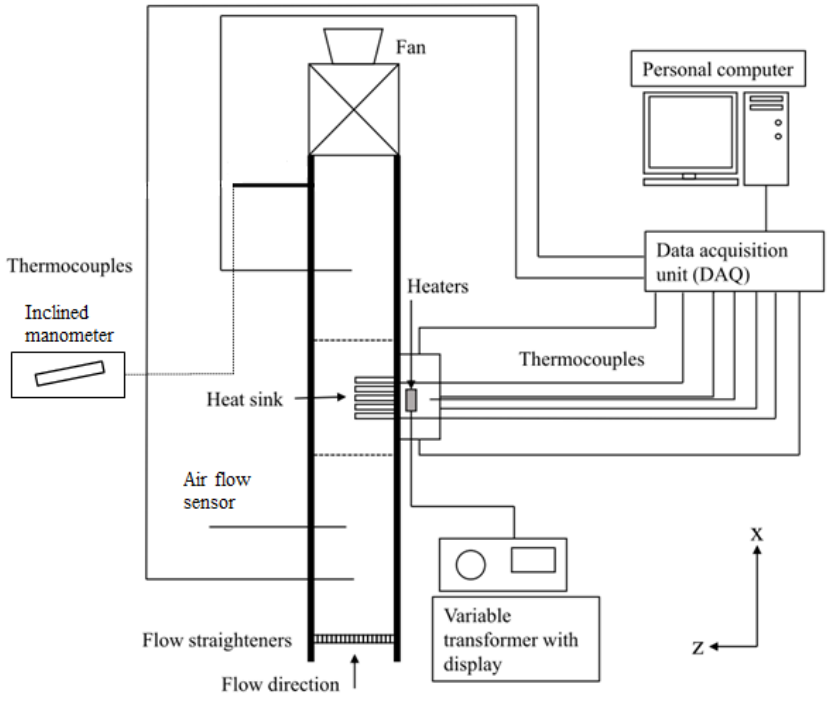

Figure 4. Microscopic views of (a) circular, (b) rectangular rounded and (c) aerofoil fins.

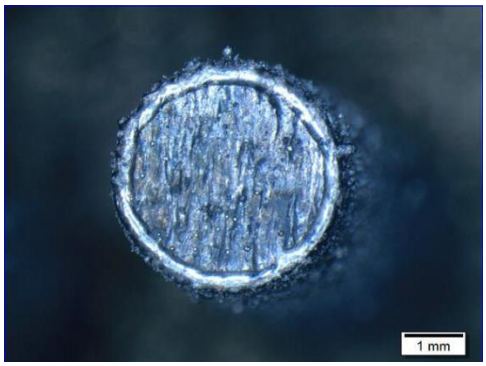

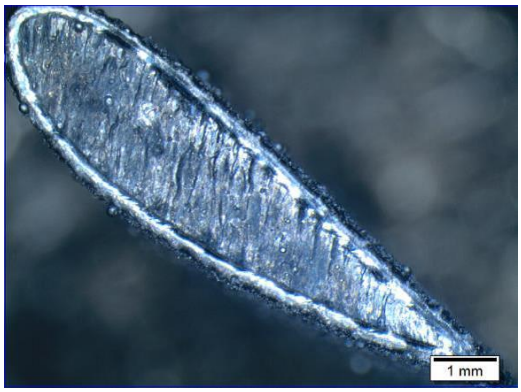

Figure 5. Nu_b vs Re of SLM fabricated heat sinks of various fin geometries

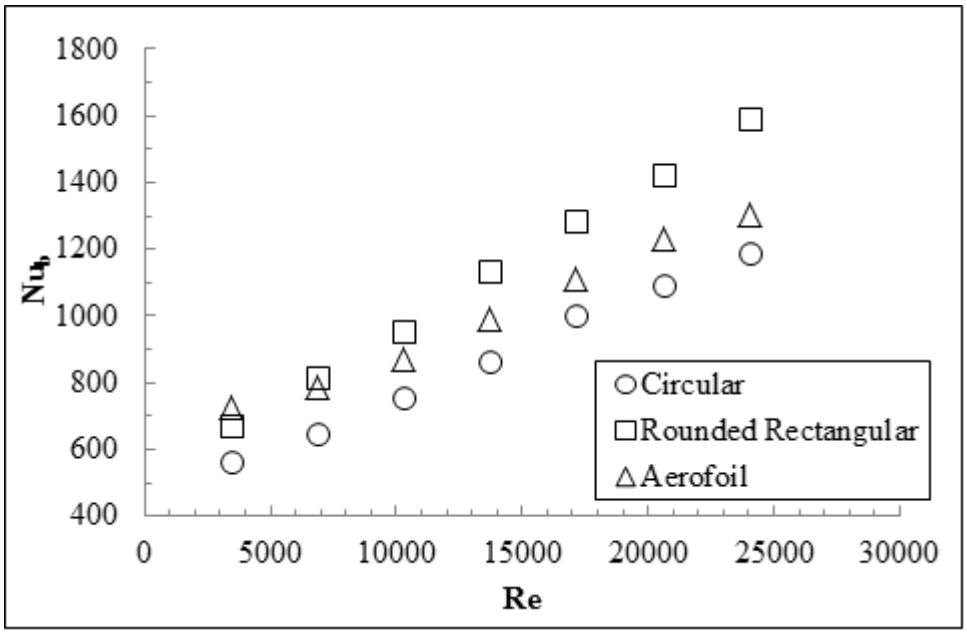

Figure 6. Nu_t vs Re of SLM fabricated heat sinks of various fin geometries

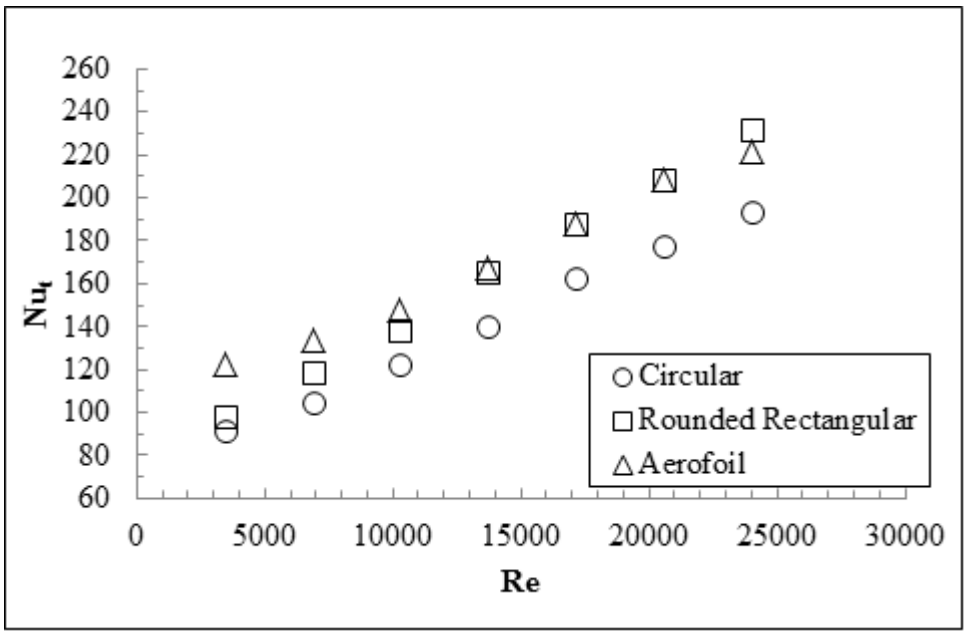

Figure 7. Illustration of vortex formation on the trailing edge of the rectangular rounded pin fin in mini smoke wind tunnel at air speed of 1.5 m/s.